Potential Energy Surfaces for the S_1-S_0 Relaxation of *trans*-Diphenyldiphosphene in the P═P Rotation-Restricted Condition

Yoshiaki Amatatsu†

Faculty of Engineering and Resource Science, Akita University, Tegata Gakuen-cho, Akita 010-8502, Japan

Received: March 12, 2009; Revised Manuscript Received: June 12, 2009

The potential energy surfaces (PESs) for the S_1-S_0 relaxation of *trans*-diphenyldiphosphene (DPP) in the P═P rotation-restricted condition have been calculated by means of ab initio complete active space self-consistent field and its second-order perturbation methods. Two types of PESs for the S_1-S_0 relaxation under P═P rotation-restricted condition have been scanned, starting from the stable geometry in S_1 where the two phenyl groups are perpendicularly twisted against the P═P part. The nonsymmetric inversion route where one of the CPP parts takes a linear geometry is favorable. On the other hand, the symmetric inversion route where both the ∠CPP angles increase simultaneously is energetically unfavorable. This is contrastive with the case of azobenzene (AZB) in the N═N rotation-restricted condition. It has been confirmed that the discussion for the photochemistry of DPP is also true for a realistic diphosphene protected by a bulky substituent. The electronic factors on the shapes of PESs for the nonsymmetric inversion and the symmetric inversion routes of DPP have been analyzed and compared with those of AZB.

1. Introduction

Multiple bond compounds of heavier main group elements have been of great interest in the basic chemistry as well as the material science.[1–3] For the last several years, especially, this class of compounds has been intended to be utilized as photofunctional materials.[4–6] The idea of the applications to new photofunctional materials is based on the small HOMO−LUMO energy gaps of multiple bond compounds, which make it possible to tune the absorption and emission properties. In order to exploit excellent photofunctional materials, a further characterization of the excited states is desirable, although the P═P bonding nature in the ground state has been studied.[7] Very recently we gave a new insight about the excited states of diphenyldiphosphene (PhP═PPh, Ph, phenyl group) (denoted by DPP hereafter) which is an analogue of azobenzene (PhN═NPh) (denoted by AZB).[8] Though the electronic structures of DPP are similar to those of AZB, the potential energy surface (PES) in S_1 with respect to the phenyl torsions is quite different from that of AZB. At the stable geometry of DPP in S_1 around the Franck−Condon region (denoted by S_1-geometry(90)), two phenyl groups of DPP are perpendicularly twisted against the P═P part (i.e., $\phi \sim \phi' \sim 90°$ and $\tau \sim 180°$ in Figure 1). At the stable geometry of AZB in S_1 (S_1-geometry(C_{2h})), on the other hand, AZB takes a planar structure with C_{2h} symmetry (i.e., $\phi = \phi' = 0°$ and $\tau = 180°$). This implies that the photochemical behavior of DPP is different from that of AZB. In the present paper, we focus our interest on the S_1-S_0 relaxation process of DPP where the P═P rotation is restricted spatially, in comparison with that of AZB.

The S_1-S_0 relaxation process of AZB has been extensively studied experimentally[9–24] as well as theoretically,[25–30] although it is still controversial. A common feature of the photochemical behavior upon S_1 excitation is that the quantum yield is almost constant (∼0.25) independent of the surroundings.[9,10] Contrary to the independence of the quantum yield on the surroundings, the lifetime in S_1 is strongly dependent on them. In *n*-hexane,

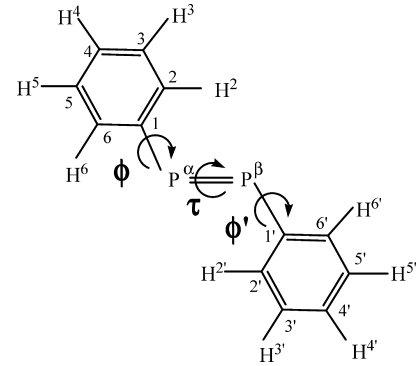

Figure 1. Numbering of atoms in DPP. The bending angles of $\angle C^1P^\alpha P^\beta$ and $\angle C^{1'}P^\beta P^\alpha$ are denoted by α and β. The dihedral angles of $\angle C^1P^\alpha P^\beta C^{1'}$, $\angle C^2C^1P^\alpha P^\beta$, and $\angle P^\alpha P^\beta C^{1'}C^{2'}$ are denoted by τ, ϕ, and ϕ'. The similar definitions of the numbering of atoms and the internal coordinates in AZB are made.

the fluorescence exhibits biphasic decay;[12,13,16,18,19,22,23] the time constants for the shorter and longer components are 0.34 and 3.0 ps, respectively.[18] The biphasic decays are also found in the photochemistry of substituted azobenzenes.[11,17,20,24] In case that the N═N rotation is restricted in viscous solvent of ethylene glycol, within a cyclodextrin cavity, or with a chemical modification by cyclophane or crown ether, it also exhibits biphasic decay, but the longer time constant is much larger.[14,15,22,23] In order to explain the lifetime dependent on the surroundings, it is proposed that AZB in S_1 takes different routes for the relaxation into S_0. In the former case (i.e., *n*-hexane) which allows the N═N rotation, AZB in S_1 takes a "rotation" route by twisting the N═N bond for the relaxation into S_0. The temporal behavior of the fluorescence depolarization supports this route.[21] In addition, the PESs by high levels of quantum mechanical calculations support the rotation route.[25–29] In the latter cases that the surroundings prevent the N═N rotation, there are two possible S_1-S_0 relaxation routes of AZB, schematically shown in Figure 2. One candidate is "nonsymmetric inversion" route where the inversion about one N atom

† E-mail: amatatsu@ipc.akita-u.ac.jp. Fax: 81-18-889-2601.

10.1021/jp902217h CCC: $40.75
Published on Web 08/12/2009

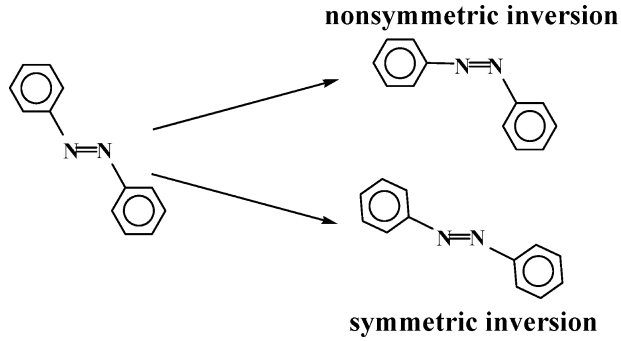

Figure 2. Possible routes in S_1 for the S_1-S_0 relaxation of AZB in the N=N rotation-restricted condition.

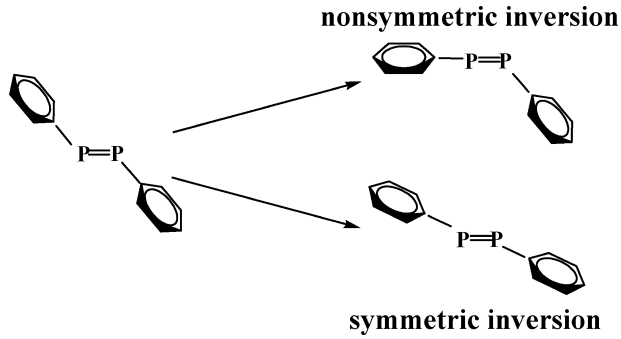

Figure 3. Possible routes from the S_1-geometry(90) in S_1 for the S_1-S_0 relaxation of DPP in the P=P rotation-restricted condition.

takes place in the same molecular plane. By quantum mechanical calculations, it is found that the S_1 and S_0 PESs do not cross each other in case that one of the ∠CNN angles is large but the other is kept small.[26,28,29] Another candidate is a "symmetric inversion" route where the two ∠CNN angles simultaneously increase in the same molecular plane. The S_1 and S_0 PESs with respect to the symmetric increase of the two ∠CNN angles cross each other at ∠CNN ∼ 157° where the energy is above the stable geometry in S_1 by 0.92 eV (21.2 kcal/mol).[26] The temporal behavior of the fluorescence depolarization modestly also supports the symmetric inversion route.[21] Here we note that the "nonsymmetric inversion" and "symmetric inversion" in our present paper are referred as "inversion" and "concerted inversion" in some cases.[21,22,26]

Concerning the S_1-S_0 relaxation routes of DPP from the stable S_1-geometry(90) of DPP under P=P rotation-restricted condition, there are at least two possible relaxation routes schematically shown in Figure 3. So our present concern is about the PESs along the nonsymmetric inversion and the symmetric inversion routes from the S_1-geometry(90). Thereby, we try to characterize the P=P double bond from a viewpoint of the excited state, in comparison with the N=N double bond of AZB.

The present paper is organized as follows. In the next section, we describe the computational strategy for the present calculation. In section 3, we discuss the PESs of DPP and AZB along the nonsymmetric inversion and the symmetric inversion routes. Then we examine the electronic effects on the shapes of the PESs so as to extract the characteristics of the P=P double bond. Furthermore, we make comment on the S_1-S_0 relaxation process of realistic diphosphenes protected by a bulky substituent. Last of all, we give a summary on the present computational results and future perspective of the photochemistry of diphosphenes.

2. Method of Calculations

In the present calculations, we took a computational strategy the same as our previous one.[8] A complete active space self-consistent field (CASSCF) calculation where all the nine π-type occupied orbitals (including two nonbonding orbitals on the P atoms) and the lowest seven unoccupied π^* orbitals are taken into account (denoted by (18,16)CASSCF) is desirable but impractical to scan the global PESs for the S_1-S_0 relaxation process of DPP. So we preliminarily performed configuration interaction (CI) calculations where up to triple excitations from the Hartree−Fock configuration were taken into account. Thereby, it is found that at most the highest five π occupied and the lowest five π^* unoccupied orbitals as well as two nonbonding orbitals on the P atoms are enough to describe our present interest of S_0 and S_1 states at any geometries which possibly contribute to the photochemistry of DPP. So we adopted 14 electrons in 12 orbitals CASSCF ((14,12)CASSCF) for scanning of the global PESs. In necessity, we made correction for (14,12)CASSCF energy of each electronic state using the second-order multireference Möller−Plesset perturbation (MRMP2) method where all valence and virtual orbitals were included.

First we scanned the PESs of the nonsymmetric inversion and the symmetric inversion routes (see Figure 3). As mentioned later, the nonsymmetric inversion route is more realistic in the S_1-S_0 relaxation of DPP under constraint that the P=P rotation is restricted spatially. Then we determined the conical intersection between S_1 and S_0 (S_1/S_0-CIX) to examine the inversion route in detail. Here we determined the S_1/S_0-CIX by a smaller (8,5)CASSCF method because the S_1/S_0-CIX region is well described by the four highest occupied MOs (HOMOs) and the lowest unoccupied MO (LUMO). After the determination of S_1/S_0-CIX by (8,5)CASSCF, however, we performed the present standard (14,12)CASSCF calculation at the S_1/S_0-CIX to verify that the energy difference between S_1 and S_0 is small enough to be a CIX. This implies that a much more computationally demanding (14,12)CASSCF gives an S_1/S_0-CIX similar to that by (8,5)CASSCF.

Then we also did similar calculations (i.e., scanning of the PESs for the S_1-S_0 relaxation routes in Figure 2) of AZB by (14,12)CASSCF and MRMP2 methods. Thereby, we compare the photochemistry of DPP with that of AZB under N=N rotation-restricted condition.

In order to confirm that the discussion on the photochemistry of DPP is valid for a realistic diphosphene of which the P=P part is protected by a bulky substituent, we performed similar calculations of bis(2,6-dimethylphenyl)diphosphene by (14,12)-CASSCF and MRMP2 methods.

In the scanning of the PESs, we used the GAMESS program in the present ab initio calculations with the Huzinaga−Dunning double-ζ basis set augmented by polarizations ($\alpha_d = 0.75$ for C atoms, $\alpha_d = 0.55$ for P atoms, and $\alpha_d = 0.80$ for N atoms).[31] In the determination of the S_1/S_0-CIX for the inversion route of DPP, we used Gaussian03 with a smaller basis set where the polarization function is augmented only on the P atoms.[32]

3. Results and Discussion

3.1. S_1-S_0 Relaxation Routes of DPP. Figure 4a shows the PESs of the nonsymmetric inversion route, which were obtained as a function of the $\angle C^1P^\alpha P^\beta$ bending angle α where the other parameters in S_1 are optimized under constraint that DPP has C_s symmetry and the two phenyl groups are perpendicularly twisted. In this route, the S_1 state is not so destabilized even at a large α, while the S_0 state is destabilized so as to be close to the S_1 state. Then we calculated the PESs in the region around $\alpha = 180°$ in order to determine another important internal coordinate for the surface crossing between S_1 and S_0. Figure

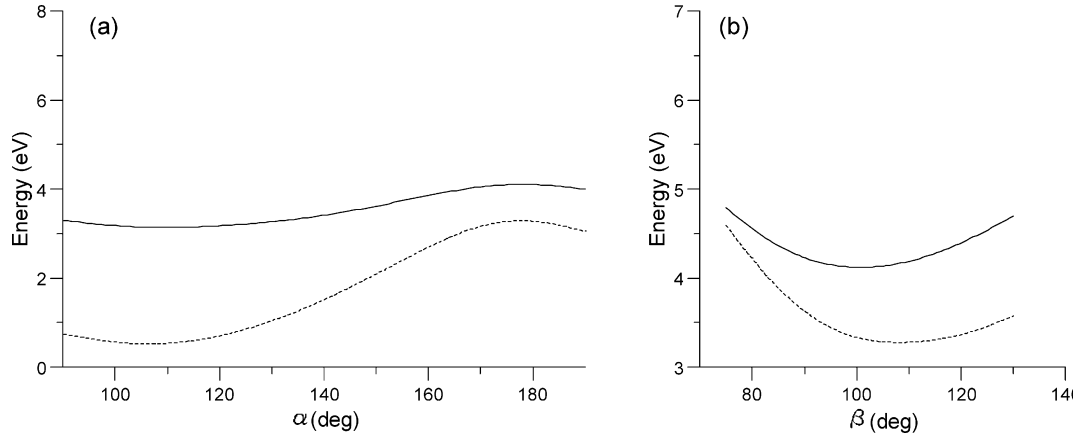

Figure 4. Potential energy surfaces (PESs) for the nonsymmetric inversion route of DPP: the solid lines are for S_1, and the dotted lines are for S_0. (a) The PESs are obtained as a function of α where the other geometrical parameters are optimized in S_1 under the constraint that DPP has C_s symmetry and the two phenyl groups are perpendicularly twisted against the P═P part. (b) The PESs are obtained as a function of β where α is fixed to 180° and the two phenyl groups are perpendicularly twisted but the remaining parameters are optimized in S_1. The energy in S_0 is evaluated at each optimized geometry in S_1. Note that the α > 180° of the abscissa corresponds to the cis-form region. The energy scale of the ordinate in panel b is half that of panel a.

TABLE 1: Characteristic Optimized Parameters at Important Conformations of DPP and AZB

DPP	S_0-geometry[a]	S_1-geometry-(90)[a]	S_1/S_0-CIX	S_1/S_0-CIX-(sym)[b]
	Bond Distances (angstroms)			
$P^{\alpha}P^{\beta}$	2.056	2.153	2.217	1.957
$P^{\alpha}C^{1}$	1.834	1.821	1.817	1.810
$P^{\beta}C^{1'}$	1.834	1.821	1.858	1.810
	Bond Angles (deg)			
$\alpha(C^{1}P^{\alpha}P^{\beta})$	103.1	109.0	168.3	172.0
$\beta(C^{1'}P^{\beta}P^{\alpha})$	103.1	109.0	74.8	172.0
	Dihedral Angles (deg)			
$\tau(C^{1}P^{\alpha}P^{\beta}C^{1'})$	−177.9	−179.1	0.0	180.0
$\phi(C^{2}C^{1}P^{\alpha}p^{\beta})$	30.3	89.6	90.6	92.2
$\phi'(C^{2'}C^{1'}P^{\beta}P^{\alpha})$	30.3	89.6	92.2	92.2

AZB	S_0-geometry[a]	S_1-geometry(C_{2h})[a]	S_1/S_0-CIX(sym)[c]
	Bond Distances (angstroms)		
$N^{\alpha}N^{\beta}$	1.246	1.257	1.217
$N^{\alpha}C^{1}$	1.426	1.369	1.347
$N^{\beta}C^{1'}$	1.426	1.369	1.347
	Bond Angles (deg)		
$\alpha(C^{1}N^{\alpha}N^{\beta})$	114.8	128.4	154.5
$\beta(C^{1'}N^{\beta}N^{\alpha})$	114.8	128.4	154.5
	Dihedral Angles (deg)		
$\tau(C^{1}N^{\alpha}N^{\beta}C^{1'})$	180.0	180.0	180.0
$\phi(C^{2}C^{1}N^{\alpha}N^{\beta})$	0.0	0.0	0.0
$\phi'(C^{2'}C^{1'}N^{\beta}N^{\alpha})$	0.0	0.0	0.0

[a] The values are taken from ref 8. The S_1-geometry(90) was referred as the S_1-geometry in ref 8. [b] The S_1/S_0-CIX(sym) of DPP is a crossing point for the symmetric inversion route in Figure 5. [c] The S_1/S_0-CIX(sym) of AZB is a crossing point for the symmetric inversion route in Figure 7.

4b shows the PESs as a function of the other $\angle C^{1'}P^{\beta}P^{\alpha}$ bending angle β where α is fixed to 180° and the remaining parameters are optimized in S_1. From this figure, it is found that a large α (∼180°) and a small β (∼75°) are essential to surface crossing between S_1 and S_0. Actually, the S_1/S_0-CIX is located in this region by means of a smaller (8,5)CASSCF with a smaller basis set (refer to Table 1). We checked the energy difference between S_1 and S_0 by the present standard (14,12)CASSCF method at the S_1/S_0-CIX. As seen in Table 2, the energy difference (0.014 eV) is small enough to be a CIX even by (14,12)CASSCF. This

TABLE 2: Electronic Structures of DPP at S_1/S_0-CIX

	energy (eV)[a]	dipole moment (debye)	main CSFs[b]
S_0	4.816	1.333	0.885 (closed shell)
S_1	4.802	2.049	0.910 (1−1′)

[a] The energies in S_0 and S_1 at S_1/S_0-CIX are not exactly same. This is because the S_1/S_0-CIX geometry is optimized by (8,5)CASSCF but the energies in this table are evaluated by the present standard (14,12)CASSCF. [b] The CSFs (configuration state functions) of which absolute values of CI coefficients are greater than 0.3 are listed. The seven occupied π orbitals (including two nonbonding orbitals) and the lowest five unoccupied π^* ones in the order of energy are designated by 7, 6, 5, 4, 3, 2, 1 (HOMO), 1′ (LUMO), 2′, 3′, 4′, 5′, respectively. 1−1′ in the parentheses, for instance, indicates the CSF of single excitation from orbital 1 to 1′.

implies that an S_1/S_0-CIX by a terribly computationally demanding (14,12)CASSCF is similar to the S_1/S_0-CIX by (8,5)CASSCF with a smaller basis set.

Our next concern is how electronically excited DPP travels from S_0-geometry into S_1/S_0-CIX. Although the intrinsic reaction coordinate analysis or molecular dynamics simulation is desirable to obtain detailed information, we examined it by an easier approach of two types of geometry optimizations in S_1 from S_0-geometry and S_1/S_0-CIX, respectively. Both of the optimizations substantially give the stable geometry in S_1 around the Franck−Condon region (denoted by S_1-geometry(90) in Table 1) where the two phenyl groups are almost perpendicularly twisted against the P═P part. This implies that the route of S_0-geometry → S_1-geometry(90) → S_1/S_0-CIX is likely. Concerning the geometrical change of S_0-geometry → S_1-geometry(90) in S_1, we can easily deduce from Table 1 and the S_1 gradients with respect to the internal coordinates. The S_1 gradients of the P═P stretch, the ∠CPP bending, and the phenyl torsion are large at S_0-geometry (−0.035, −0.047, and −0.004 au, respectively). This means the initial events upon electronic excitation into S_1 at the S_0-geometry are the elongation of the P═P bond, the enlargement of the ∠CPP angles, and the phenyl torsion toward the perpendicularly twisted conformation. In comparison of the S_0-geometry with the S_1-geometry(90) in Table 1, it is found that the initial events in S_1 directly connect the S_0-geometry with the S_1-geometry(90). In the second stage of S_1-geometry → S_1/S_0-CIX, the asymmetrization of the two ∠CPP angles (α and β) is important, while the other parameters remain almost unchanged. One of the ∠CPP angles, α, increases to take a linear

TABLE 3: Energies (eV) at Important Conformations of DPP and AZB

DPP	S_0-geometry[a]	S_1-geometry-(90)	S_1/S_0-CIX	S_1/S_0-CIX-(sym)
S_0	0.0 (0.0)[b]		4.816 (4.107)	7.458 (6.812)
S_1	3.544 (2.759)	3.125 (2.577)	4.802 (4.014)	7.469 (6.503)

AZB	S_0-geometry[a]	S_1-geometry(C_{2h})	S_1/S_0-CIX(sym)
S_0	0.0 (0.0)		3.631 (3.439)
S_1	3.277 (2.412)	2.718 (1.888)	3.629 (2.807)

[a] The values are taken from ref 8. [b] The numbers in the parentheses are the MRMP2 values.

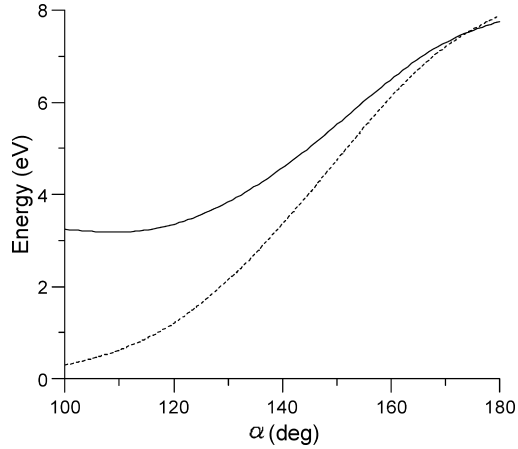

Figure 5. Potential energy surfaces (PESs) for the symmetric inversion route of DPP: the solid lines are for S_1, and the dotted lines are for S_0. The PESs are obtained as a function of α where the two phenyl groups are perpendicularly twisted against the P═P part and the other geometrical parameters are optimized in S_1 under constraint of C_{2h} symmetry at the phenyl perpendicularly twisted conformation. The energy in S_0 is evaluated at the optimized geometry in S_1 for each α.

shape of the $C^1P^\alpha P^\beta$ part, while the other, β, decreases to access the S_1/S_0-CIX.

Here we briefly mention the reliability of the energies before further discussion on the PESs of the photochemical process. Table 3 lists the energies at important conformations by CASSCF and MRMP2 methods. The MRMP2 energies are lower by 0.5−0.7 eV than the CASSCF energies irrespective of the conformations. This implies that the shapes of PESs by MRMP2 are similar to those by (14,12)CASSCF. The MRMP2 energy in S_1 at S_0-geometry (2.759 eV) is in good agreement with the experimental absorption maximum (2.695 eV; 460 nm) of a realistic diphosphene protected by a bulky substituent.[33] From these computational findings, our present standard (14,12)CASSCF is reliable enough to discuss the photochemistry but the MRMP2 energies are proper for the comparison with the experimental values. From now on, we refer the MRMP2 values as for the energies. In the first process of S_0-geometry → S_1-geometry(90), DPP in S_1 is stabilized, but in the second process of S_1-geometry(90) → S_1/S_0-CIX, DPP is much destabilized by ∼1.44 eV.

Figure 5 shows the PESs of the symmetric inversion route, where the two ∠CPP angles, α and β, take a same value but the other geometrical parameters are optimized under constraint of C_{2h} at the phenyl perpendicularly twisted conformations. It is found that the S_1 and S_0 surfaces cross at a large ∠CPP bending angle $\alpha = \beta \sim 172°$, but the energy at the crossing point (i.e., S_1/S_0-CIX(sym)) is much higher (∼2.5 eV) than that at the S_1/S_0-CIX for the nonsymmetric inversion route. This implies that the nonsymmetric inversion route is more realistic than that of the symmetric inversion route for the S_1-S_0 relaxation in the P═P rotation-restricted condition.

3.2. S_1-S_0 Relaxation Routes of AZB. Though the PESs of the S_1-S_0 relaxation routes of AZB in the N═N rotation-restricted condition have been already reported by several authors,[26,28,29] we also scanned the PESs for the routes in Figure 2 in order to compare with the S_1-S_0 relaxation routes of DPP. The nonsymmetric inversion PESs in Figure 6a are obtained as a function of $\angle C^1N^\alpha N^\beta$ angle α where the other geometrical parameters are optimized in S_1 under constraint of C_s symmetry at $\phi = \phi' = 0.0°$. The symmetric inversion PESs in Figure 7 is obtained by a similar way under constraint of C_{2h} symmetry. Here we note that the starting S_0-geometry of AZB is planar (see the relevant part of AZB in Table 1) and that AZB in S_1 maintains a planar conformation in both cases of the symmetric and nonsymmetric inversion routes. Contrary to the case of DPP, the S_1 state for the symmetric inversion route is not so destabilized even at a large ∠CNN angle α, while the S_0 state is quickly destabilized as increase of α. This leads to surface crossing between S_1 and S_0 in low energy at a large α. In the nonsymmetric inversion route, the shapes of the S_1 and S_0 PESs are similar to those of DPP in Figure 4a. So we further examined the PESs around the $\alpha = 180°$ region as a function of the other $\angle C^{1'}N^\beta N^\alpha$ angle β. Figure 6b shows the PESs as a function of β where α is fixed to 180° and the remaining geometrical parameters are optimized in S_1 under constraint of C_s symmetry. It is found that the S_1 and S_0 PESs cross each other in a large-β region, leading to the same crossing point for the symmetric inversion.

3.3. Electronic Factors. In the previous subsections, we found out that the nonsymmetric inversion route of DPP is favorable for the S_1-S_0 relaxation under P═P rotation-restricted condition, whereas the symmetric inversion route is favorable in the case of AZB. So we examine the electronic factors on the shapes of the PESs for the different S_1-S_0 relaxation routes. Concerning the first processes (i.e., S_0-geometry → S_1-geometry(90) for DPP, S_0-geometry → S_1-geometry(C_{2h}) for AZB) after electronic excitation into S_1, we discussed the details in our previous paper.[8] However, we make a brief review on them (refer to Table 4). In the case of DPP, the electron in the 3s and the in-plane 3p (i.e., $3p_x + 3p_y$) orbitals decreases from 0.937, 2.116 into 0.892, 1.784, respectively, while the electron in the out-of-plane $3p_z$ increases from 0.994 into 1.397. This is ascribed to the fact that the electronic excitation into S_1 is $n-\pi^*$. In the process of S_0-geometry → S_1-geometry(90) in S_1, the electron in the 3s and the in-plane 3p orbitals on the P atoms increases into 0.915, 1.802, while that on the $3p_z$ orbital (1.402) little changes. As analyzed in our previous paper, the increase of the 3s and the in-plane 3p electron on the P atoms is due to an effective interaction of the nonbonding orbitals in the P═P part with the π orbitals over the phenyl groups, which leads to S_1-geometry(90) where the two phenyl groups are perpendicularly twisted against the P═P part (i.e., $\phi \sim \phi' \sim 90°$). In the case of AZB, on the other hand, the out-of-plane $2p_z$ electron decreases from 1.370 into 1.350 in the process of S_0-geometry to S_1-geometry(C_{2h}) (refer to Table 5). This is due to the enhancement of the π conjugation between the N═N part and the phenyl groups. In other words, the π electron over the N═N part is more delocalized entirely over a molecule in S_1, which geometrically reflects shrinking of the linkage CN bonds (1.426 Å at S_0-geometry, 1.369 Å at S_1-geometry(C_{2h})) in the AZB part of Table 1.

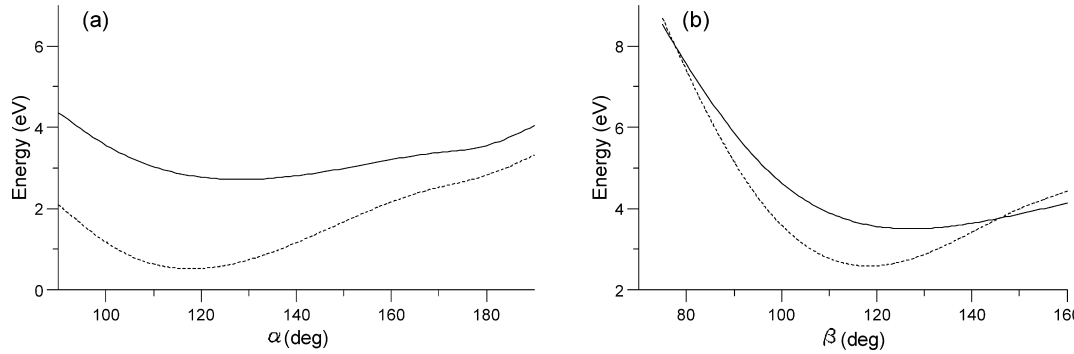

Figure 6. Potential energy surfaces (PESs) for the nonsymmetric inversion route of AZB: the solid lines are for S_1, and the dotted lines for S_0. (a) The PESs are obtained as a function of α where the other geometrical parameters are optimized in S_1 under constraint of planar structure. (b) The PESs are obtained as a function of β where α is fixed to 180° but the remaining parameters are optimized in S_1. The energy in S_0 is evaluated at the optimized geometry in S_1. Note that the α > 180° of the abscissa corresponds to the cis-form region.

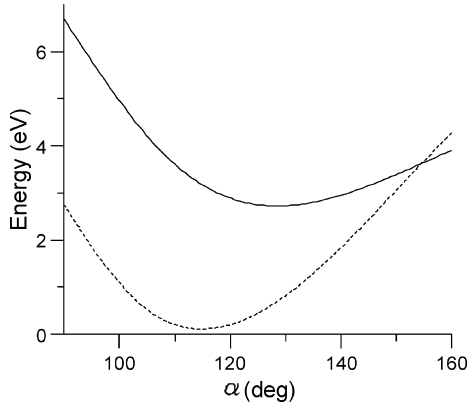

Figure 7. Potential energy surfaces (PESs) for the symmetric inversion route of AZB: the solid lines are for S_1, and the dotted lines are for S_0. The PESs are obtained as a function of α where the other geometrical parameters are optimized in S_1 under constraint of C_{2h} symmetry at $\phi = \phi' = 0°$. The energy in S_0 is evaluated at the optimized geometry in S_1 for each α.

Now we discuss the second steps starting from the stable geometries in S_1 around the Franck−Condon region (i.e., S_1-geometry(90) for DPP and S_1-geometry(C_{2h}) for AZB, respectively). In the process of S_1-geometry(90) → S_1/S_0-CIX where the two ∠CPP angles α and β are asymmetrized, the electron in the in-plane 3p (i.e., $3p_x + 3p_y$) orbitals on the P^α atom increases from 1.802 into 1.916, while that on the P^β atom decreases into 1.709 (see Table 4). The out-of-plane $3p_z$ electron on each P atom exhibits a same trend (i.e., increase from 1.402 into 1.584 on the P^α atom, decrease from 1.402 into 1.195 on the P^β atom, respectively). In other words, the 3p (i.e., $3p_x$, $3p_y$, and $3p_z$) electron over the P═P part is populated evenly on both the P^α and P^β atoms around the S_1-geometry(90). In the asymmetrization process of α and β (i.e., nonsymmetric inversion route), however, the 3p electron turns to be populated mainly on the P^α atom which relates to the larger ∠CPP angle. Furthermore, the sums of the in-plane 3p (i.e., $3p_x + 3p_y$) and the out-of-plane $3p_z$ electron on the P═P part at the S_1/S_0-CIX (1.916 + 1.709 = 3.625 for the in-plane 3p, 1.584 + 1.195 = 2.779 for $3p_z$) are similar to those at S_1-geometry(90) (1.802 × 2 = 3.604 for the in-plane 3p, 1.402 × 2 = 2.804 for $3p_z$), respectively. This implies that the 3p electron on the P^β relating to the smaller $\angle C^{1'}P^\beta P^\alpha$ angle β transfers into the 3p orbitals on the P^α with the large $\angle C^1P^\alpha P^\beta$ angle α, which successfully escape from the electronic repulsion arising from the highly crowded local geometry around the P^β atom. The interpretation of the electron transfer from the P^β into the P^α atom is valid at least for the case of the out-of-plane $3p_z$ electron. However, we do not interpret that the change of the in-plane 3p electron population is due to the electron transfer from the P^β into the P^α atom. The 3s electron on the P^α and P^β atoms exhibits a trend opposite to the case of the 3p electron (i.e., decrease from 0.915 into 0.824 for the P^α atom, increase from 0.915 into 0.996 for the P^β atom). Furthermore, the sum of the 3s and in-plane 3p electron on each atom at S_1/S_0-CIX (i.e., 2.740 for P^α, 2.705 for P^β) is not different from that at the S_1-geometry(90) (i.e., 2.717 for both the P^α and P^β atoms), respectively. So we interpret the change of the in-plane 3p electron population as follows. In the process of S_1-geometry(90) → S_1/S_0-CIX, the electron on the P^β atom favors to be populated in a smaller space of the 3s orbital rather than in a more spacious in-plane 3p orbital because of a highly crowded geometry around the P^β atom, while the electron on the P^α atom favors to be populated in a more spacious 3p orbital because of a large $\angle C^1P^\alpha P^\beta$ angle. In other words, the in-plane 3p electron on the P^β atom is confined into the 3s orbital, while that on the P^α atom moves out from the 3s orbital. That is, we interpret that the changes of the electron populations in the 3s and the in-plane 3p orbital are due to the rehybridization on each P^β and P^α atom, not to the charge transfer from the P^β into the P^α atoms. In conclusion, the highly distorted S_1/S_0-CIX is energetically stabilized in two ways: the out-of-plane $3p_z$ electron transfer from the P^β into the P^α atom and the rehybridizations among the 3s and in-plane 3p electron on each P atom.

We confirm that such an electronic factor for the distorted S_1/S_0-CIX is not found in the symmetric inversion process of S_1-geometry(90) → S_1/S_0-CIX(sym) which is energetically unfavorable. As seen in the relevant part of Table 4, the out-of-plane $3p_z$ electron remains almost unchanged (from 1.402 to 1.382). The 3s electron decreases from 0.915 to 0.744, while the in-plane 3p (i.e., $3p_x + 3p_y$) electron increases from 1.802 into 2.196. The change of the 3s and the in-plane 3p electron can be interpreted by the same reason for the case of the P^α atom with the larger $\angle C^1P^\alpha P^\beta$ angle in the nonsymmetric inversion route. In comparison with the electronic factor for the nonsymmetric inversion route, the following factors are missing in the symmetric inversion route: the π electron transfer from the P^β onto the P^α atom and the confinement of the in-plane 3p electron into the 3s orbital on the P^β atom. In other words, these factors are important for the stabilization of the distorted S_1/S_0-CIX.

In turn we examine the electronic factors for the S_1-S_0 relaxation process of AZB under N═N rotation-restricted condition. As mentioned in section 3.2., the symmetric inversion is energetically favorable. Table 5 lists the electron populations

TABLE 4: Electron Populations at Important Conformations of DPP

geometry	S_0-geometry[a]		S_1-geometry(90)[a]	S_1/S_0-CIX	S_1/S_0-CIX(sym)
state	S_0	S_1	S_1	S_1	S_1
atomic orbitals on P					
3s	0.937	0.892	0.915	0.824 (0.996)[b]	0.744
$3p_x$[c]	0.837	0.857	0.866	0.920 (0.726)	0.871
$3p_y$[c]	1.279	0.926	0.936	0.996 (0.983)	1.325
in-plane 3p ($3p_x + 3p_y$)[c]	2.116	1.784	1.802	1.916 (1.709)	2.196
$3p_z$[b]	0.994	1.397	1.402	1.584 (1.195)	1.382
net charge on P	0.252	0.246	0.207	0.075 (0.375)	0.103

[a] The values in columns of S_0-geometry (for S_0 and S_1) and of S_1-geometry(90) (for S_1) are different from those in columns of $\phi = 30°$ (for S_0 and S_1) and $\phi = 90°$ (for S_1) in Table 5 of ref 8. The former are the values at S_0-geometry and S_1-geometry(90) in Table 1. On the other hand, the latter are the values at slightly different geometries. That is, the geometries in columns of $\phi = 30°$ and $\phi = 90°$ were obtained by setting to $\phi = 30°$ and 90°, where the other geometrical parameters are fixed to those of planar S_0-geometry with C_{2h} (denoted by (S_0-geometry(C_{2h}) in ref 8). As commented in the footnote of Table 5 in ref 8, this was to see the phenyl torsional angle dependence only. However, even in the present case of the fully optimized S_0-geometry and S_1-geometry(90), a similar discussion can be done as in the text. [b] Due to the asymmetric angles of α and β at the S_1/S_0-CIX, the electron population on the P^β atom in the parentheses is different from that on the P^α atom. [c] The directions of *x*-, *y*-, and *z*-axes are determined by diagonalizing the tensor of the moment of inertia. The *z*-axes for all the geometries are designed to be the out-of-plane π orbitals over the P═P bond, whereas the *x*- and *y*-axes are the in-plane orbitals such as the nonbonding orbitals.

TABLE 5: Electron Populations at Important Conformations of AZB

geometry	S_0-geometry[a]		S_1-geometry(C_{2h})	S_1/S_0-CIX(sym)	α = 180, β = 78[b]
state	S_0	S_1	S_1	S_1	S_1
atomic orbitals on N					
2s	0.914	0.883	0.853	0.796	0.833 (1.040)[c]
$2p_x$[d]	1.158	1.050	1.074	1.032	1.079 (0.958)
$2p_y$[d]	1.380	1.153	1.178	1.323	1.145 (1.174)
in-plane 2p ($2p_x + 2p_y$)[d]	2.538	2.203	2.252	2.356	2.223 (2.132)
$2p_z$[d]	0.996	1.370	1.350	1.321	1.502 (1.248)
net charge on N	−0.049	−0.044	−0.033	−0.044	−0.104 (−0.038)

[a] The values are taken from ref 8. [b] The geometry of α = 180, β = 78 corresponds to the crossing point in Figure 6b. [c] Due to the asymmetric angles of α and β, the electron population on the N^β atom in the parentheses is different from that on the N^α atom. [d] The directions of *x*-, *y*-, and *z*-axes are determined by diagonalizing the tensor of the moment of inertia. The *z*-axes for all the geometries are designed to be the out-of-plane π orbitals over the N═N bond, whereas the *x*- and *y*-axes are the in-plane orbitals such as the nonbonding orbitals.

at important conformations of AZB. In the process of S_1-geometry(C_{2h}) → S_1/S_0-CIX(sym), the electron flow of the 2s, in-plane 2p (i.e., $2p_x + 2p_y$), and out-of-plane $2p_z$ orbitals exhibits a trend similar to the case of the symmetric inversion of DPP. Nevertheless, the energy at the S_1/S_0-CIX(sym) of AZB (2.81 eV) is much lower than that of DPP (6.50 eV). A clue for this difference is the net charges on the N and P atoms. In both cases, the N or P atoms becomes more negatively charged in the symmetric inversion process (from −0.033 to −0.044 for AZB in Table 5, from 0.207 to 0.103 for DPP in Table 4), which is ascribed to the electron transfer from the phenyl groups. In the case of AZB, this electron transfer into the N═N part is energetically favorable because the N atom is more electronegative than the C^1 and $C^{1'}$ atoms. On the other hand, the electron transfer into the P═P part is unfavorable in the case of DPP because of the more electropositive P atoms.

Before terminating the present paragraph, we summarize the electronic effects on the shapes of the PESs of DPP and AZB. In the case of AZB, the symmetric inversion is energetically favorable. This is because a large ∠CNN angle with C_{2h} symmetry serves the electron to flow into the more electronegative N═N part so that the S_1 state is not so destabilized even at large ∠CNN angles. In the case of DPP, the nonsymmetric inversion route is favorable. The S_1/S_0-CIX takes a highly distorted geometry where one of the ∠CPP angles is large, while the other is enormously small. In order to stabilize the highly distorted S_1/S_0-CIX in S_1, two types of the electronic reorganizations take place on the nonsymmetric inversion PES of S_1-geometry(90) → S_1/S_0-CIX. One is the π electron transfer over the P═P bond so as to escape from the electronic repulsion at a crowded geometry around the P^β atom with a small $\angle C^{1'}P^\beta P^\alpha$ angle. The other is the rehybridizations of the 3s and the in-plane 3p orbitals on each P atom. On the P^β atom with a small $\angle C^{1'}P^\beta P^\alpha$ angle, the electrons in the spacious in-plane 3p orbitals are confined into the 3s orbital. On the P^α atom with a large $\angle C^1P^\alpha P^\beta$ angle, the 3s electron moves out to the more spacious 3p orbitals. These rehybridizations are characteristic of the P═P bond and not found in the N═N bond of AZB (refer to the relevant part (α = 180, β = 78) in Table 5).

3.4. S_1-S_0 Relaxation Process of Realistic Diphosphene. In the previous subsections, we pointed out that the nonsymmetric inversion route of DPP is energetically favorable more than the symmetric inversion route for the S_1-S_0 relaxation in the P═P rotation-restricted condition. In order to validate the discussion on the S_1-S_0 relaxation route of DPP, we performed additional calculations of a realistic diphosphene protected by a bulky 2,6-dimethylphenyl group more than phenyl group. Table 6 lists the characteristic optimized geometrical parameters of bis(2,6-dimethylphenyl)diphosphene (DMPDP). It is found that the two 2,6-dimethyphenyl groups of DMPDP are perpendicularly twisted against the P═P bond even in S_0 ($\phi = \phi' = 91.8°$), which is ascribed to a bulky substituent effect so as for DMPDP to escape from a steric repulsion with the P═P part. This is in agreement with experimental and computational findings.[33,34] In other words, DMPDP is a proper model for real diphosphenes. Furthermore, two following computational findings also validate that DMPDP is a proper model for the photochemistry of real diphosphenes to be discussed. The

TABLE 6: Characteristic Optimized Parameters at Important Conformations of DMPDP

DMPDP	S_0-geometry	S_1-geometry
Bond Distances (angstroms)		
$P^{\alpha}P^{\beta}$	2.051	2.146
$P^{\alpha}C^{1}$	1.854	1.830
$P^{\beta}C^{1'}$	1.854	1.830
Bond Angles (deg)		
$\alpha(C^{1}P^{\alpha}P^{\beta})$	101.2	109.7
$\beta(C^{1'}P^{\beta}P^{\alpha})$	101.2	109.7
Dihedral Angles (deg)		
$\tau(C^{1}P^{\alpha}P^{\beta}C^{1'})$	179.8	175.8
$\phi(C^{2}C^{1}P^{\alpha}P^{\beta})$	91.8	92.8
$\phi'(C^{2'}C^{1'}P^{\beta}P^{\alpha})$	91.8	92.8

TABLE 7: Energies (eV) at Important Conformations of DMPDP

DMPDP	S_0-geometry	S_1-geometry-(90)	S_1/S_0-CIX[a]	S_1/S_0-CIX-(sym)[a]
S_0	0.0 (0.0)[b]		4.710 (3.789)	6.866 (6.147)
S_1	3.232 (2.605)	2.938 (2.428)	4.793 (3.848)	7.081 (6.025)

[a] The geometrical parameters of the S_1/S_0-CIX and S_1/S_0-CIX(sym) are commented on in the text. [b] The numbers in the parentheses are the MRMP2 values.

excitation energies of DMPDP (2.605 eV in Table 7) well reproduce the experimental absorption maximum of 2.695 eV, 460 nm.[32] The S_1-geometry(90), which is similar to that of DPP, is not different from the S_0-geometry (refer to Table 6). This rationalizes the experimental findings of the Raman excitation profile.[35]

The S_1/S_0-CIX and S_1/S_0-CIX(sym) of DMPDP were not fully optimized. Instead the geometrical parameters of the DPP parts of DMPDP were taken from those of DPP which were fully optimized (refer to Table 1). The geometrical parameters of the remaining methyl groups were taken from those of the S_0-geometry of DMPDP because the geometrical parameters of the methyl groups at the S_1-geometry(90) are similar to those at the S_0-geometry in Table 6. As seen in Table 7, the energy differences between S_1 and S_0 are kept small at the S_1/S_0-CIX and S_1/S_0-CIX(sym) of DMPDP. The energy at the S_1/S_0-CIX (ca. 3.85 eV) is much lower than that at the S_1/S_0-CIX(sym) even in the case of DMPDP (ca. 6.03 eV). This means that the nonsymmetric inversion route of DMPDP is energetically favorable more than the symmetric inversion route, as in the case of bare DPP.

On the basis of these computational findings, we make comment on the S_1-S_0 relaxation process of realistic diphosphenes protected by a bulky substituent in the P═P rotation-restricted condition. One point is that this relaxation process is substantially the same as the second process of bare DPP discussed above. The only difference is that the first process where the phenyl groups are twisted from 30° to 90° is missing in the case of realistic diphosphenes such as DMPDP, because the bulky 2,6-dimethylphenyl groups are perpendicularly twisted against the P═P part even in S_0 due to a steric repulsion. Another point is that the energies at the S_1/S_0-CIXs are higher by ca. 1.25 eV than those in S_1 at S_0-geometry irrespective of protection by bulky substituents or not (refer to Tables 3 and 7). This is much higher than the case of AZB (ca. 0.40 eV in Table 3). For the present, we have two interpretations for the high-energy location of the S_1/S_0-CIX since there are no experimental findings concerning the S_1-S_0 relaxation process in the P═P rotation-restricted condition. One interpretation is that realistic diphosphenes in S_1 hardly decay into S_0 and are more fluorescent than AZB in the P═P or N═N rotation-restricted condition. Another interpretation is that the P═P rotation which is completely ignored in the present study plays an important role even in the P═P rotation-restricted condition, as predicted by molecular dynamic simulation of N═N rotation-restricted azobenzene derivatives of azobenzenophanes.[30]

4. Concluding Remarks

In the present paper we theoretically characterized the P═P double bond from a viewpoint of the S_1-S_0 relaxation processes of DPP and realistic diphosphene in the P═P rotation-restricted condition, in comparison with the N═N double bond of AZB. In the case of DPP, the nonsymmetric inversion route where one of the two ∠CPP angles increases to a linear geometry of the CPP part is energetically favorable more than the symmetric inversion route where both the ∠CPP angles increase. This is contrastive with the case of AZB where the symmetric inversion is favorable. The difference of the S_1-S_0 relaxation PESs can be rationalized by two factors. One is the difference of the stable geometries in S_1 around the Franck−Condon region. In the case of DPP, the phenyl groups are perpendicularly twisted due to the effective interaction between the nonbonding orbitals on the P atoms and the phenyl groups. In the case of AZB, on the other hand, the phenyl torsion is more impeded from a planar geometry due to the increase of the π bond character in the linkage CN bond. The other is the flexibility of the P═P double bond which allows DPP to take a highly distorted S_1/S_0-CIX with asymmetric ∠CPP angles. The π electron over the P═P bond becomes easily populated on the P atom relating to the larger ∠CPP angle in order to avoid the electronic repulsion between the P═P part and the phenyl group relating to the smaller ∠CPP angle. The 3s and the in-plane 3p orbitals easily cause rehybridization. On the P atom relating to the smaller ∠CPP angle, the in-plane 3p electron is confined into the smaller 3s orbital, while the 3s electron moves out to the more spacious 3p orbitals on the other P atom in relation to the larger ∠CPP angle. This kind of rehybridization is not seen in the case of AZB with an N═N bond.

Following our previous paper,[8] we characterized the P═P double bond from a viewpoint of the excited state in the present one. Thereby, we found that the PESs of diphosphenes for the S_1-S_0 relaxation process in the P═P rotation-restricted condition are quite different from those of AZB. Our next concern is about the PESs for the S_1-S_0 relaxation of diphosphenes in the P═P rotation-free condition. In the case of the N═N rotation-free condition of AZB, the N═N rotation easily takes place so as for AZB to directly reach an S_1/S_0-CIX at the dihedral angle ∠CNNC ∼ 90°.[25−29] Furthermore, it is pointed out that the S_1-S_0 relaxation via the N═N rotation can take place even in the case of the azobenzenophanes where the N═N rotation is thought to be blocked.[30] So we checked if realistic diphosphene protected by a bulky substituent (i.e., bis(2,4,6-tri-*tert*-butylphenyl)diphosphene) reaches a perpendicularly twisted (i.e., the dihedral angle ∠CPPC ∼ 90°) conformation by a simple P═P twist of the molecular model in hand. A simple twist of the P═P bond of this realistic diphosphene causes an unfavorable contact between the *tert*-butyl groups, whereas that of unrealistic DPP without any bulky substituent does not. On the basis of a speculation with the molecular model, we imagine a story different from the case of AZB. That is, realistic diphosphenes reach an S_1/S_0-CIX at the dihedral angle ∠CPPC ∼ 90° not via a direct P═P rotation but via an indirect route, even if possible. We are now in progress of the scanning of the PESs relating to the S_1-S_0 relaxation route under P═P rotation-free condition.

Acknowledgment. This work is financially supported by Grant-in-Aid for Priority Area (Molecular Theory for Real Systems) (Nos.19029004 and 20038004) from the Ministry of Education, Culture, Sports, Science and Technology.

References and Notes

(1) Weber, L. *Chem. Rev.* **1992**, *92*, 1839–1906.
(2) Power, P. P. *Chem. Rev.* **1999**, *99*, 3463–3503.
(3) Mathey, F. *Angew. Chem., Int. Ed.* **2003**, *42*, 1578–1603.
(4) Wright, V. A.; Gates, D. P. *Angew. Chem., Int. Ed.* **2002**, *41*, 2389–2392.
(5) Smith, R. C.; Protasiewicz, J. D. *J. Am. Chem. Soc.* **2004**, *126*, 2268–2269.
(6) Kawasaki, S.; Nakamura, A.; Toyota, K.; Yoshifuji, M. *Bull. Chem. Soc. Jpn.* **2005**, *78*, 1110–1120.
(7) Cowley, A. H.; Decken, A.; Norman, N. C.; Krüger, C.; Lutz, F.; Jacobsen, H.; Ziegler, T. *J. Am. Chem. Soc.* **1997**, *119*, 3389–3390.
(8) Amatatsu, Y. *J. Phys. Chem. A* **2008**, *112*, 8824–8828.
(9) Botolus, P.; Monti, S. *J. Phys. Chem.* **1979**, *83*, 648–652.
(10) Rau, H.; Lüddecke, E. *J. Am. Chem. Soc.* **1982**, *104*, 1616–1620.
(11) Wachtveitl, J.; Nägele, T.; Puell, B.; Zinth, W.; Krüger, M.; Rudolph-Böhner, S.; Oesterhelt, D.; Moroder, L. *J. Photochem. Photobiol., A* **1997**, *105*, 283–288.
(12) Nägele, T.; Hoche, R.; Zinth, W.; Wachtveitl, J. *Chem. Phys. Lett.* **1997**, *272*, 489–495.
(13) Lednev, I. K.; Ye, T.-Q.; Matousek, P.; Towrie, M.; Foggi, P.; Neuwahl, F. V. R.; Umapathy, S.; Hester, R. E.; Moore, J. N. *Chem. Phys. Lett.* **1998**, *290*, 68–74.
(14) Lednev, I. K.; Ye, T.-Q.; Abbott, L. C.; Hester, R. E.; Moore, J. N. *J. Phys. Chem. A* **1998**, *102*, 9161–9166.
(15) Fujino, T.; Tahara, T. *J. Phys. Chem. A* **2000**, *104*, 4203–4210.
(16) Fujino, T.; Arzhantsef, S. Y.; Tahara, T. *J. Phys. Chem. A* **2001**, *105*, 8123–8129.
(17) Hirose, Y.; Yui, H.; Sawada, T. *J. Phys. Chem. A* **2002**, *106*, 3067–3071.
(18) Satzger, H.; Spörlein, S.; Root, C.; Wachtveitl, J.; Zinth, W.; Gilch, P. *Chem. Phys. Lett.* **2003**, *372*, 216–223.
(19) Satzger, H.; Root, C.; Braun, M. *J. Phys. Chem. A* **2004**, *108*, 6265–6271.
(20) Schmidt, B.; Sobotta, C.; Mulkmas, S.; Laimgruber, S.; Braun, M.; Zinth, W.; Gilch, P. *J. Phys. Chem. A* **2004**, *108*, 4399–4404.
(21) Chang, C.-W.; Lu, Y.-C.; Wang, T.-T.; Diau, E. W.-G. *J. Am. Chem. Soc.* **2004**, *126*, 10109–10118.
(22) Lu, W.-C.; Diau, E. W.-G.; Rau, H. *J. Phys. Chem. A* **2005**, *109*, 2090–2099.
(23) Pancur, T.; Renth, F.; Temps, F.; Harbaum, B.; Krüger, A.; Herges, R.; Näther, Chr. *Phys. Chem. Chem. Phys.* **2005**, *7*, 1985–1989.
(24) Poprawa-Smoluch, M.; Baggerman, J.; Zhang, H.; Maas, H. P. A.; De Cola, L.; Brouwer, A. M. *J. Phys. Chem. A* **2006**, *110*, 11926–11937.
(25) Ishikawa, T.; Noro, T.; Shoda, T. *J. Chem. Phys.* **2002**, *115*, 7503–7512.
(26) Diau, E. W.-G. *J. Phys. Chem. A* **2004**, *108*, 950–956.
(27) Cembran, A.; Bemardi, F.; Garavelli, M.; Gagliardi, L.; Orlandi, G. *J. Am. Chem. Soc.* **2004**, *126*, 3234–3243.
(28) Tiago, M. L.; Ismail-Beigi, S.; Louie, S. G. *J. Chem. Phys.* **2005**, *122*, 094311/1–7.
(29) Crecca, C. R.; Roitberg, A. E. *J. Phys. Chem. A* **2006**, *110*, 8188–8203.
(30) Ciminelli, C.; Granucci, G.; Persico, M. *J. Chem. Phys.* **2005**, *123*, 174317/1–10.
(31) Schmidt, M. W.; Baldridge, K. K.; Boatz, J. A.; Elbert, S. T.; Gordon, M. S.; Jensen, J. H.; Koseki, S.; Matsunaga, N.; Nguyen, K. A.; Su, S. J.; Windus, T. L.; Dupuis, M.; Montgomery, J. A., Jr. *J. Comput. Chem.* **1993**, *14*, 1347–1363.
(32) Frisch, M. J.; Trucks, G. W.; Schlegel, H. B.; Scuseria, G. E.; Robb, M. A.; Cheeseman, J. R.; Montgomery, J. A., Jr.; Vreven, T.; Kudin, K. N.; Burant, J. C.; Millam, J. M.; Iyengar, S. S.; Tomasi, J. J.; Barone, V.; Mennucci, B.; Cossi, M.; Scalmani, G.; Rega, N.; Petersson, G. A.; Nakatsuji, H.; Hada, M.; Ehara, M.; Toyota, K.; Fukuda, R.; Hasegawa, J.; Ishida, M.; Nakajima, T.; Honda, Y.; Kitao, O.; Nakai, H.; Klene, M.; Li, X.; Knox, J. E.; Hratchian, H. P.; Cross, J. B.; Adamo, C.; Jaramillo, J.; Gomperts, R.; Stratmann, R. E.; Yazyev, O.; Austin, A. J.; Cammi, R.; Pomelli, C.; Ochterski, J. W.; Ayala, P. Y.; Morokuma, K.; Voth, A.; Salvador, P.; Dannenberg, J. J.; Zakrzewski, V. G.; Dapprich, S.; Daniels, A. D.; Strain, M. C.; Farkas, O.; Malick, D. K.; Rabuck, A. D.; Raghavachari, K.; Foresman, J. B.; Ortiz, J. V.; Cui, Q.; Baboul, A. G.; Clifford, S.; Cioslowski, J.; Stefanov, B. B.; Liu, G.; Liashenko, A.; Piskorz, P.; Komaromi, I.; Martin, R. L.; Fox, D. J.; Keith, T.; Al-Laham, M. A.; Peng, C. Y.; Nanayakkara, A.; Challacombe, M.; Gill, P. M. W.; Johnson, B.; Chen, W.; Wong, M. W.; Gonzalez, C.; Pople, J. A. Gaussian 03, revision B.04; Gaussian, Inc.: Pittsburgh, PA, 2003.
(33) Hamaguchi, H.; Tasumi, M.; Yoshifuji, M.; Inamoto, N. *J. Am. Chem. Soc.* **1984**, *106*, 508–509.
(34) Sasamori, T.; Takeda, N.; Tokitoh, N. *J. Phys. Org. Chem.* **2003**, *16*, 450–462.
(35) Copeland, T.; Shea, M. P.; Milliken, M. C.; Smith, R. C.; Protasiewicz, J. D.; Simpson, M. C. *Anal. Chim. Acta* **2003**, *496*, 155–163.

JP902217H